ARTHRITIS & RHEUMATISM
Vol. 63, No. 5, May 2011, pp 1301–1311
DOI 10.1002/art.30280


# A Novel *N*-ethyl-*N*-nitrosourea–Induced Mutation in *Phospholipase Cγ2* Causes Inflammatory Arthritis, Metabolic Defects, and Male Infertility In Vitro in a Murine Model

Koichiro Abe,[1] Helmut Fuchs,[2] Auke Boersma,[2] Wolfgang Hans,[2] Philipp Yu,[3] Svetoslav Kalaydjiev,[4] Matthias Klaften,[2] Thure Adler,[4] Julia Calzada-Wack,[2] Ilona Mossbrugger,[2] Birgit Rathkolb,[5] Jan Rozman,[6] Cornelia Prehn,[2] Miriam Maraslioglu,[3] Yoshie Kametani,[7] Shin Shimada,[7] Jerzy Adamski,[2] Dirk H. Busch,[4] Irene Esposito,[2] Martin Klingenspor,[6] Eckhard Wolf,[5] Wolfgang Wurst,[8] Valerie Gailus-Durner,[2] Matilda Katan,[9] Susan Marschall,[2] Dian Soewarto,[2] Sibylle Wagner,[2] and Martin Hrabě de Angelis[10]

***Objective.*** **It is difficult to identify a single causative factor for inflammatory arthritis because of the multifactorial nature of the disease. This study was undertaken to dissect the molecular complexity of systemic inflammatory disease, utilizing a combined approach of mutagenesis and systematic phenotype screening in a murine model.**

***Methods.*** **In a large-scale *N*-ethyl-*N*-nitrosourea mutagenesis project, the *Ali14* mutant mouse strain was established because of dominant inheritance of spontaneous swelling and inflammation of the hind paws. Genetic mapping and subsequent candidate gene sequencing were conducted to find the causative gene, and systematic phenotyping of *Ali14*/+ mice was performed in the German Mouse Clinic.**

***Results.*** **A novel missense mutation in the *phospholipase Cγ2* gene (*Plcg2*) was identified in *Ali14*/+ mice. Because of the hyperreactive external entry of calcium observed in cultured B cells and other in vitro experiments, the *Ali14* mutation is thought to be a novel gain-of-function allele of *Plcg2*. Findings from systematic screening of *Ali14*/+ mice demonstrated various phenotypic changes: an abnormally high T cell:B cell**

Supported in part by the Japan Society for the Promotion of Science (JSPS grants 19500370 and 22500392 to Dr. Abe) and by the Research Foundation Itsuu Laboratory (Dr. Abe), by the Nationales Genomforschungsnetz Deutschland (NGFN-Plus grants 01GS0850, 01GS0851, and 01GS0852 to Drs. Busch, Wolf, and Hrabě de Angelis), by the Deutsches Human Genome Projekt (grant-in-aid to Dr. Hrabě de Angelis), and by the European Commission (grant LSHG-2006-037188 to Dr. Hrabě de Angelis).

[1]Koichiro Abe, PhD: Tokai University School of Medicine, Kanagawa, Japan and Helmholtz Zentrum München–German Research Center for Environmental Health, Neuherberg, Germany; [2]Helmut Fuchs, PhD, Auke Boersma, DVM (current address: University of Veterinary Medicine Vienna, Vienna, Austria), Wolfgang Hans, PhD, Matthias Klaften, DVM, Julia Calzada-Wack, MD, Ilona Mossbrugger, DVM, Cornelia Prehn, PhD, Jerzy Adamski, PhD, Irene Esposito, MD, Valerie Gailus-Durner, PhD, Susan Marschall, PhD, Dian Soewarto, PhD, Sibylle Wagner, DVM: Helmholtz Zentrum München–German Research Center for Environmental Health, Neuherberg, Germany; [3]Philipp Yu, MD, Miriam Maraslioglu: Philipps-Universität Marburg, Marburg, Germany; [4]Svetoslav Kalaydjiev, MD, Thure Adler, DVM, Dirk H. Busch, MD: Helmholtz Zentrum München–German Research Center for Environmental Health, Neuherberg and Technische Universität München, Munich, Germany; [5]Birgit Rathkolb, DVM, Eckhard Wolf, DVM: Helmholtz Zentrum München–German Research Center for Environmental Health, Neuherberg, and Ludwig-Maximilians-Universität München, Munich, Germany; [6]Jan Rozman, PhD, Martin Klingenspor, PhD: Technische Universität München, Weihenstephan Campus, Freising-Weihenstephan, Germany; [7]Yoshie Kametani, PhD, Shin Shimada, PhD: Tokai University School of Medicine, Kanagawa, Japan; [8]Wolfgang Wurst, PhD: Helmholtz Zentrum München–German Research Center for Environmental Health, Neuherberg, Technische Universität München, Munich, Max Planck Institute of Psychiatry, Munich, and Deutsches Zentrum für Neurodegenerative Erkankungen, Munich, Germany; [9]Matilda Katan, PhD: Royal Cancer Hospital, London, UK; [10]Martin Hrabě de Angelis, PhD: Helmholtz Zentrum München–German Research Center for Environmental Health, Neuherberg, and Technische Universität München, Weihenstephan Campus, Freising-Weihenstephan, Germany.

Address correspondence to Koichiro Abe, PhD, Division of Basic Medical Science and Molecular Medicine, Tokai University School of Medicine, Shimokasuya 143, Isehara, Kanagawa 259-1193, Japan (e-mail: abeko@is.icc.u-tokai.ac.jp); or to Martin Hrabě de Angelis, PhD, Institute of Experimental Genetics, Helmholtz Zentrum München, German Research Center for Environmental Health, Ingolstaedter Landstrasse 1, 85764 Neuherberg, Germany (e-mail: hrabe@helmholtz-muenchen.de).

Submitted for publication August 20, 2010; accepted in revised form January 25, 2011.

**ratio, up-regulation of Ig, alterations in body composition, and a reduction in cholesterol and triglyceride levels in peripheral blood. In addition, spermatozoa from *Ali14*/+ mice failed to fertilize eggs in vitro, despite the normal fertility of the *Ali14*/+ male mice in vivo.**

***Conclusion*. These results suggest that the *Plcg2*-mediated pathways play a crucial role in various metabolic and sperm functions, in addition to initiating and maintaining the immune system. These findings may indicate the importance of the *Ali14*/+ mouse strain as a model for systemic inflammatory diseases and inflammation-related metabolic changes in humans.**

Inflammatory arthritis, including rheumatoid arthritis, often leads to significant destruction of articular tissue, resulting in physical disability (1). The disease is associated not only with immobility, but also with cachexia and depression (2). These impairments obviously cause social isolation and lead to diminishing health-related quality of life. Despite the accumulated evidence regarding systemic inflammatory diseases, only treatments targeting symptoms are available. Inflammatory arthritis is a multifactorial disease that is induced by complex combinations of genetic and environmental influences. Thus, characterization of a single factor triggering spontaneous inflammation is a major challenge in the field.

Phosphoinositide-specific phospholipase C (PLC) is a signal transduction effector involving various cell functions (3). PLC hydrolyzes phosphatidylinositol 4,5-triphosphate, a component of the plasma membrane, and generates second messenger molecules, inositol 1,4,5-triphosphate ($IP_3$) and diacylglycerol (DAG) (4). DAG remains in the plasma membrane and activates protein kinase C, while $IP_3$ induces the release of calcium ions from the endoplasmic reticulum. DAG and $IP_3$ mediate transduction of the signals from highly specific receptors of hormones, neurotransmitters, antigens, and growth factors to downstream, intracellular targets. Therefore, they contribute to the regulation of various biologic functions, such as cell motility, fertilization, and immunity.

PLC enzymes consist of 13 isozymes belonging to 6 different subtypes ($\beta$, $\gamma$, $\delta$, $\epsilon$, $\eta$, and $\zeta$). *Phospholipases C$\gamma$1* and *C$\gamma$2* (*Plcg1* and *Plcg2*, respectively) have been identified as the PLC$\gamma$ subtypes (3). *Plcg1*-null embryos appear normal at embryonic day (E) 8.5 but fail to develop beyond E9 (5). This highlights the widespread importance of *Plcg1*. In contrast, *Plcg2* is most highly expressed in hematopoietic organs such as the spleen and lymph node, and it plays a key role in constructing the immune system (6,7). In human B cells, loss of *Plcg2* signaling results in an immunodeficiency syndrome called X-linked agammaglobulinemia (8). Consistent with this, *Plcg2*-knockout mice show defects in the functioning of B cells, platelets, mast cells, and natural killer (NK) cells (9). Furthermore, analysis of a spontaneous null allele of *Plcg2*, abnormal lymphatics, revealed that *Plcg2* plays an important role in separation of blood and lymphatic vessels (10). These findings indicate a crucial role of *Plcg2* signaling in initiating and maintaining the immune system.

To increase the variety of disease models, large-scale mutagenesis programs have been carried out worldwide using *N*-ethyl-*N*-nitrosourea (ENU) in mice (11) and other vertebrates. In the ENU mutagenesis project in Munich, we use the inbred C3HeB/FeJ (C3H) mouse strain for harboring mutations (12–14). This enables the analysis of complex phenotypes without the bias of polymorphic genetic interferences, such as modifier effects from genetic background (15). Recently, this forward genetics approach in mice was used for intensive study of inflammatory arthritis (16–20). In the present study, we describe a novel dominant-mutant mouse strain, *Ali14* (*Ali* for abnormal limb), representing a novel gain-of-function allele of *Plcg2*. In addition to the described abnormalities in the immune system, *Ali14*/+ mice displayed various metabolic changes and in vitro infertility. Our findings may reveal how a single mutation leads to systemic inflammatory diseases and related symptoms in humans.

## MATERIALS AND METHODS

**Mice.** The *Ali14* mutation was generated in the Munich mouse mutagenesis project, as described previously (12,14). Briefly, we injected male C3H mice (The Jackson Laboratory) intraperitoneally with ENU (Serva Electrophoresis). The *Ali14* strain is maintained by backcrossing to wild-type (WT) female C3H mice. For genetic mapping analysis, C57BL/6J (BL/6) mice (The Jackson Laboratory) were used. For systematic phenotyping at the German Mouse Clinic, 74 mice were obtained from *Ali14*/+ and C3H WT mating pairs. The mice were genotyped by direct sequencing of polymerase chain reaction (PCR) products using specific primers (Plcg2-ex16L, 5′-GTGAATGCTGGGGTGATGTC-3′; Plcg2-ex16R, 5′-GAGCTAAGGATGCTCAAGCC-3′).

**Genetic mapping and candidate sequencing.** Genomic DNA was extracted automatically from the tail tips of arthritic $N_2$ mice (Agowa) and genotyped using 75 single-nucleotide polymorphism (SNP) markers and matrix-assisted laser desorption ionization–time-of-flight (MALDI-TOF) mass spectrometry (Sequenom), as previously described (19). For candidate sequencing analysis, we selected PCR primers beside the coding exons of *Plcg2*, using ExonPrimer (available at

http://ihg2.helmholtz-muenchen.de/ihg/ExonPrimer.html), and pools of C3H and *Ali14*/+ genomic DNA samples were sequenced using a standard Sanger sequencing procedure (ABI3100 Genetic Analyzer, Big Dye terminator chemistry; Applied Biosystems).

**Histologic and immunohistochemical analyses.** Organs were fixed in 4% buffered formalin and embedded in paraffin for histologic examinations, and formic acid was used for decalcification of paw samples (17). Myeloperoxidase (MPO) staining and immunohistochemical analyses were performed as previously described (21).

**Clinical chemical analyses.** Plasma levels of alkaline phosphatase, aspartate amylase, creatine kinase, aspartate aminotransferase, alanine aminotransferase, ferritin, transferrin, lipase, glucose, cholesterol, triglycerides, uric acid, urea, potassium, sodium chloride, calcium, inorganic phosphate, and iron were measured using an AU 400 autoanalyzer and its adapted reagents (Olympus).

**Flow cytometry and calcium fluorimetry.** Flow cytometry was performed as previously described in detail (18,22). Briefly, cells were stained with combinations of anti-IgD, anti-B220, anti-CD44, anti-CD45, anti-CD3, anti-CD4, anti-CD62L, and anti-Ly6C and analyzed using a FACSCalibur (BD Biosciences), with results assessed using either FlowJo (Tree Star) or CellQuest Pro (BD Biosciences) software. In vitro calcium monitoring was carried out as described previously (16). Briefly, WT and mutant *Plcg2* proteins were expressed in cultured WEHI-231 B cells by retroviral transfection of *Plcg2* expression constructs, based on the MIGR1 vector. For measurements of intracellular calcium flux, cells were loaded with Fura Red (Molecular Probes) and stimulated with 5 $\mu$g/ml of goat anti-murine IgM (Star 86; Serotech). Fluorescence of the cells was detected by flow cytometry.

**Adoptive transfer of splenocytes.** Splenocytes obtained from *Ali14*/+ mice or WT littermates were labeled with carboxyfluorescein succinimidyl ester (CFSE) dye using the CellTrace CFSE Cell Proliferation Kit (Invitrogen) according to the manufacturer's guidelines. WT recipients were injected intravenously with the CFSE-labeled splenocytes ($1 \times 10^7$). Clinical scores were determined in the recipient mice up to 18 days after injection, and the mice were then killed for flow cytometric and histologic analyses.

**Dual x-ray absorptiometry (DXA) and peripheral quantitative computed tomography (QCT) analysis.** We used a pDEXA Sabre X-ray Bone Densitometer (Norland Medical Systems) for capturing various bone and fat-related parameters, as previously described (17,23,24). Briefly, the entire mouse body region was assayed with a 0.02 gm/cm$^2$ histogram averaging-width setting. Peripheral QCT analysis was carried out using Stratec XCT Research SA+ (Stratec Medizintechnik).

**Measurement of body composition by nuclear magnetic resonance (NMR) imaging.** Body composition was determined using a Burker's Whole Animal Body Composition Analyzer (Minispec Bruker), based on time-domain NMR imaging. Calibration was done using dissected lean muscle and fat tissue.

**In vitro fertilization (IVF) and sperm motility measurement.** IVF experiments were performed as described previously (25). Sperm quality was measured using an IVOS Sperm Analyzer (version 12.1c; Hamilton Research) as previously described (26). The motility (percentage of all motile spermatozoa) and progressivity (percentage of spermatozoa with a minimum velocity of $\geq$60 $\mu$m/second and straightness of $\geq$50%) were evaluated.

## RESULTS

**Identification of the *Ali14*/+ strain in the Munich ENU mutagenesis project.** The *Ali14*/+ mouse line was established in the large-scale Munich ENU mutagenesis project on the basis of dominant inheritance of swollen footpads and rubor on the ears of adult mice (Figures 1A and B and data not shown). Only male offspring were found to exhibit the phenotypes. We kept the *Ali14* mutation by backcrossing with WT C3H mice more than 10 times to reduce unrelated mutations induced by ENU. Radiographs of the hind paws of *Ali14*/+ mice showed destruction of the distal phalanges, lower bone density, and sealed joints of the phalanges (Figures 1C and D). Histologic analysis of the distal phalanges of *Ali14*/+ mice indicated the presence of inflammatory infiltrates into soft tissue and increased hematopoiesis in

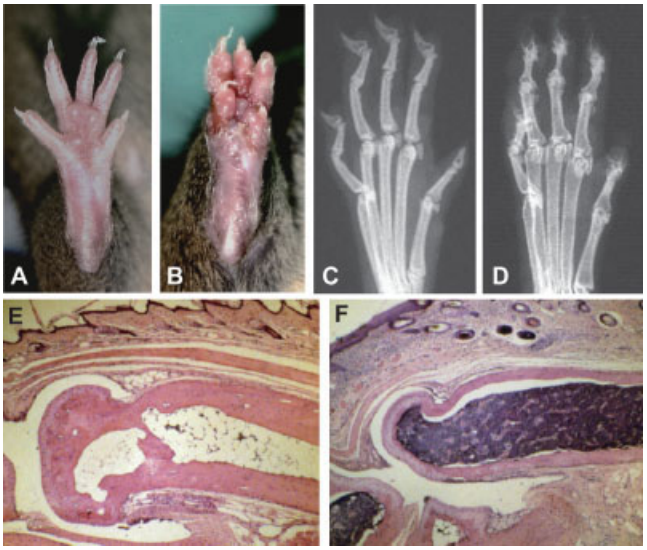


**Figure 1.** Radiographic and immunohistologic analyses of swelling and inflammation in the hind paws of *Ali14*/+ mice. **A** and **B,** Assessment of the gross morphologic appearance of the hind paws of wild-type (WT) **(A)** and *Ali14*/+ **(B)** mice indicated swollen digits and redness of the footpads in *Ali14*/+ mice. **C** and **D,** Radiographs of the hind paws of WT **(C)** and *Ali14*/+ **(D)** mice revealed destruction of the nails and distal phalanxes as well as sealed phalangeal joints in *Ali14*/+ mice. **E** and **F,** Hematoxylin and eosin staining of sections of the phalanges of WT **(E)** and *Ali14*/+ **(F)** mice demonstrated abnormally thin compact bones and increased hematopoiesis in bone marrow in the phalanges of *Ali14*/+ mice. Infiltrated inflammatory cells were also observed in the dermis. Original magnification $\times$ 5.

the bone marrow (Figures 1E and F). In addition, severe dermatitis and ulceration were observed in the ear auricles of *Ali14*/+ mice, while in the spleen, increased hematopoiesis was observed in red pulps (results available at http://abe.med.u-tokai.ac.jp/index.html or from the corresponding author upon request).

Immunohistochemical analysis using a granulocyte marker, MPO, showed that numerous positively staining cells were found in the regions of dermatitis in the ear auricles (results available from the corresponding author upon request). In contrast to the results with MPO, markers for B cells (B220), T cells (CD3), and macrophages (Mac3) stained only a minor population of the infiltrates (results not shown).

**Association of the *Ali14* mutation with an amino acid substitution in *Plcg2*.** We started genetic mapping of the *Ali14* mutation using the BL/6 mouse as a partner strain. However, none of the (C3H-*Ali14*/+ × BL/6-+/+)$F_1$ mice exhibited the inflammatory arthritis phenotype. We randomly selected the $F_1$ mice for crossing to the original WT strain, C3H-+/+, to reduce suppressive effects in the next generation. As anticipated, some of the mating pairs produced offspring with swollen paws. We subjected genomic DNA from 56 phenotype-positive mice to MALDI-TOF mass spectrometry with 75 genome-wide SNP markers. Among the 75 SNP markers, one marker, rs4227428, exhibited the highest logarithm of odds (LOD) score (LOD 2.72), and the LOD scores for all other markers were below 1.28 (Figure 2A).

The rs4227428 SNP locates on the distal region of chromosome 8. We identified *Plcg2* as a possible candidate gene in this region, because a previously identified gain-of-function mutation in the *Plcg2* gene, the *Plcg2*$^{Ali5}$ mutation, causes a similar arthritis phenotype (16). Subsequently, we identified an AT-to-GC transition in exon 16 of *Plcg2* that distinguishes C3H-+/+ and C3H-*Ali14*/+ mice (Figure 2B). DNA sequencing of the same region in WT BL/6, BALB/cByJ, CAST/EiJ, and 129SvJ mouse genomes revealed no polymorphisms (Figure 2B and results not shown).

The *Ali14* mutation causes an amino acid substitution at tyrosine-495, to a cysteine residue. Interestingly, the tyrosine residue is conserved among various vertebrates (Figure 2C). It is located not within the catalytic domain but within a split pleckstrin homology (spPH) domain that is specific to the PLCγ family (Figure 2D). Importantly, the *Ali14* mutation leads to greater responsiveness to a variety of upstream signals, such as epidermal growth factor (EGF) in vitro (27). Therefore, these observations indicate that *Ali14* is a

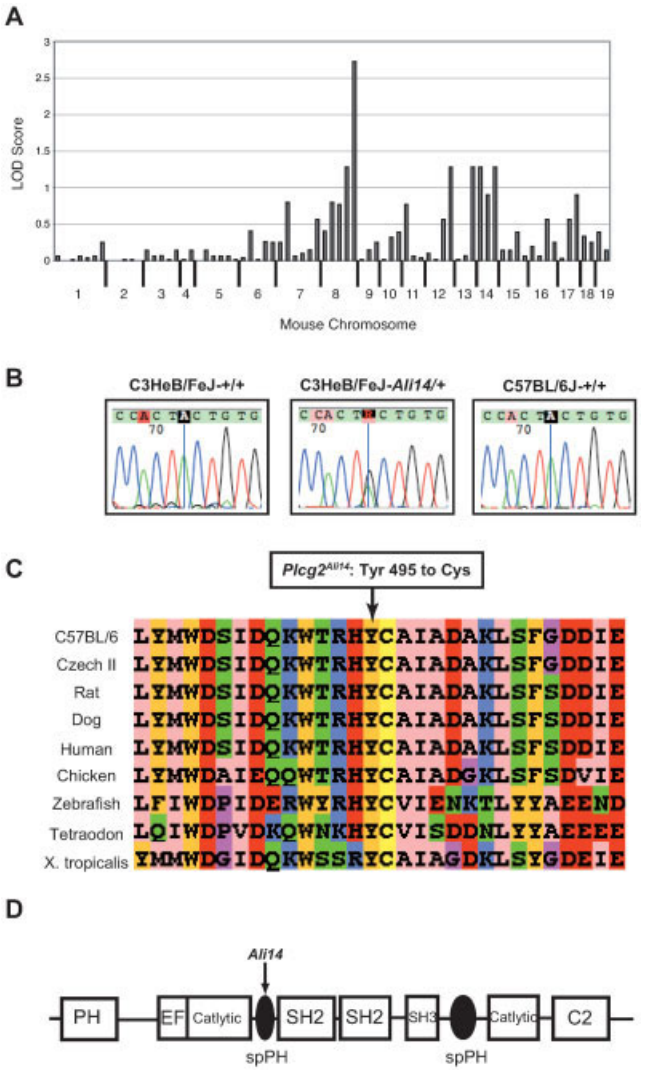


**Figure 2.** Identification of the *Ali14* mutation by positional candidate cloning. **A,** Standard genome-wide genetic mapping using single-nucleotide polymorphism markers identified the distal region of chromosome 8 as the *Ali14* candidate region, according to logarithm of odds (LOD) scores. **B,** An AT-to-GC transition on the *Ali14* genome was identified in exon 16 of the *phospholipase Cγ2* gene (*Plcg2*). **C,** Among various classes of vertebrates, the *Ali14* mutation causes an amino acid substitution ($Tyr^{495}$–Cys) **(arrow)** of *Plcg2* in conserved tyrosine. **D,** The domain structure of *Plcg2* is shown. **Arrow** indicates the position of the *Ali14* mutation. spPH = split pleckstrin homology (domain).

gain-of-function allele of *Plcg2*, and this mutation is hereafter referred to as *Plcg2*$^{Ali14}$.

**Immune system characteristics of *Plcg2*$^{Ali14/+}$ mice.** Because the functions of *Plcg2* in lymphocytes are well characterized, we analyzed the expression patterns of lymphocytes and related parameters in *Plcg2*$^{Ali14/+}$ mice. In B cell populations in the peripheral blood of

*Plcg2*$^{Ali14/+}$ mice, the frequency of IgD+B220+ double-positive cells was drastically reduced (45.5% in *Plcg2*$^{Ali14/+}$ mice versus 80.5% in WT mice) (Figure 3A). In T cell populations, the proportion of activated/memory CD44+Ly6C+ cells within the CD8 compartment was increased in *Plcg2*$^{Ali14/+}$ mouse peripheral blood (37.5%) as compared with that in WT mouse peripheral blood (16.2%) (Figure 3A). These results indicate that *Plcg2*$^{Ali14/+}$ mice display increased expression of T cells and decreased expression of B cells, as has also been detected in *Plcg2*$^{Ali5/+}$ mutant mice (16). Populations of granulocytes and NK cells were not changed (results not shown).

We also measured levels of different Ig isotypes in the plasma of *Plcg2*$^{Ali14/+}$ mice, since increased Ig levels are often observed in patients with inflammatory arthritis. Results of bioplex bead array assays demonstrated that IgG2a, IgG3, and IgA were expressed at normal levels in *Plcg2*$^{Ali14/+}$ mouse plasma (Figure 3B). However, plasma levels of IgG1, IgG2b (only in male mutants), and IgM in *Plcg2*$^{Ali14/+}$ mice were significantly increased (for IgG1 [in both sexes], $P < 0.01$ versus WT mice; for IgG2b [in males] and IgM [in both sexes], $P < 0.05$ versus WT mice) (Figure 3B). Although we measured plasma levels of autoantibodies (anti-DNA and rheumatoid factor), no significant differences were detected (results not shown).

In previous studies of *Plcg2*$^{Ali5/+}$ mice, increased and sustained external calcium entry were observed in B cells (16). Therefore, we analyzed the levels of external calcium entry using an in vitro system. We used 4 different *Plcg2* constructs, generated with either no mutation (WT-*Plcg2*), the *Ali5* mutation (*Ali5-Plcg2*), the *Ali14* mutation (*Ali14-Plcg2*), or both the *Ali5* and *Ali14* mutations (*Ali5/Ali14-Plcg2*). These constructs were introduced into cultured WEHI-231 B cells by retroviral transfection, and calcium mobilization was assayed by calcium fluorimetry. Interestingly, the cells transfected with *Ali14-Plcg2* showed the highest initial peak of calcium entry and longest duration of sustained calcium levels when compared with cells transfected with any of the other constructs (Figure 3C).

To verify the immunologic origin of the inflammatory arthritis phenotype, we performed adoptive transfer experiments in which CFSE-labeled *Ali14*/+ splenocytes were injected intravenously into WT recipients. However, no arthritis phenotype was observed to develop within 18 days after injection (n = 4), although certain numbers of CFSE-positive donor cells were detected in the lymphoid organs of the recipients, as revealed by flow cytometry (results not shown).

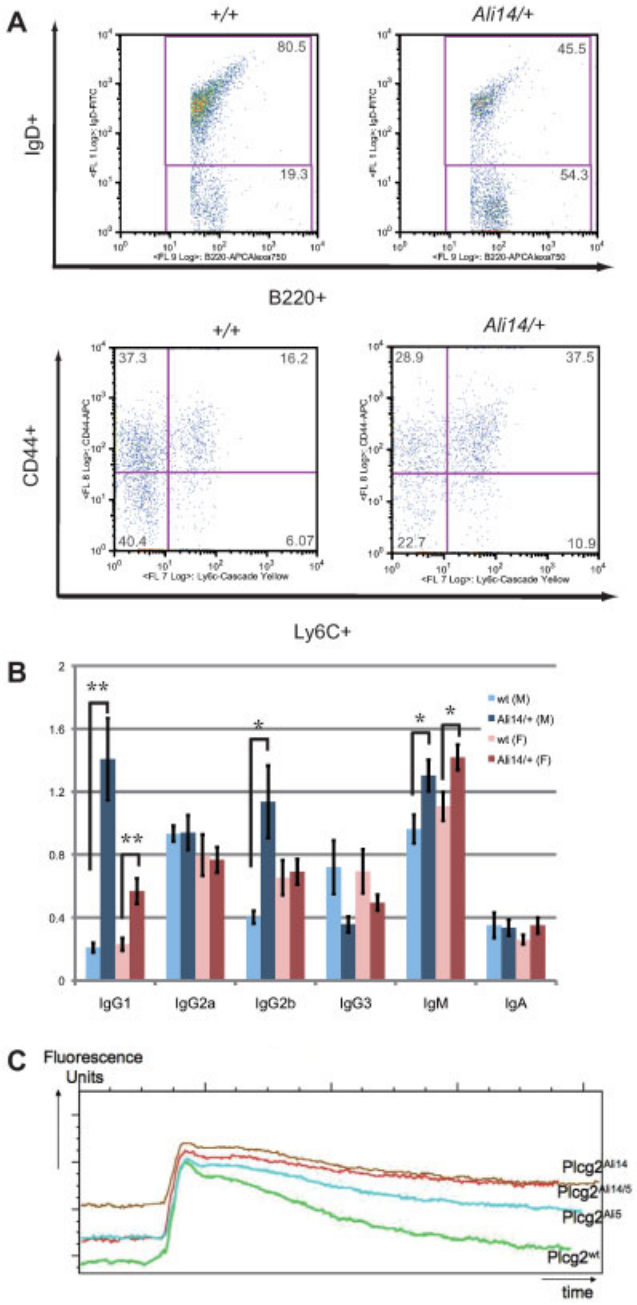


**Figure 3. A,** Lymphocyte phenotypes were assessed by flow cytometry in wild-type (WT) (+/+) and *Plcg2*$^{Ali14/+}$ mice, for populations of IgD+B220+ B cells (upper panels) and CD44+Ly6C+ T cells (lower panels). Values in each segment are the percentage of positive cells. **B,** Plasma Ig levels were determined by enzyme-linked immunosorbent assay. Bars show the mean ± SEM levels of Ig subclasses in male (M) and female (F) WT and *Plcg2*$^{Ali14/+}$ mice. * = $P < 0.05$; ** = $P < 0.01$. **C,** External calcium entry (assessed as fluorescence units over time) in a cultured B cell line was assayed by calcium fluorimetry. The MIGR1 retrovirus vector was used to introduce various *Plcg2* constructs. FITC = fluorescein isothiocyanate; APC = allophycocyanin.

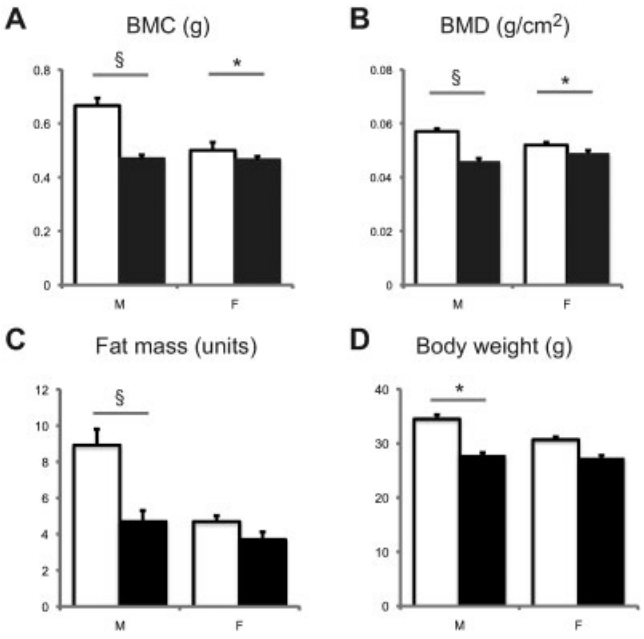


**Figure 4.** Bone- and fat-related phenotypes in male (M) and female (F) *Plcg2*$^{Ali14/+}$ mice. **A–C,** Dual x-ray absorptiometry analysis revealed reduced bone mass, measured as bone mineral content (BMC) **(A)** and bone mineral density (BMD) **(B),** as well as reduced fat mass **(C)** in *Plcg2*$^{Ali14/+}$ mice (solid bars) compared with wild-type mice (open bars). **D,** Body weight was also reduced in *Plcg2*$^{Ali14/+}$ mice. Bars show the mean ± SEM. $* = P < 0.01$; $§ = P < 0.0001$.

**Bone- and fat-related parameters in *Plcg2*$^{Ali14/+}$ mice.** To ascertain whether the phenotypes observed in *Plcg2*$^{Ali14/+}$ mice were limited to the peripheral paws or were a systemic feature in the body, we used DXA analysis. Although results from DXA are of semiquantitative quality, DXA enables a fast scan of whole-body composition. As shown in Figures 4A and B, *Plcg2*$^{Ali14/+}$ mice displayed significantly reduced bone mineral content and bone mineral density as compared to that in WT mice of both sexes (both $P < 0.0001$ in males and $P < 0.01$ in females).

We next used peripheral QCT to characterize the bone phenotype of *Plcg2*$^{Ali14/+}$ mice in more detail. In the distal femoral metaphysis, total bone density and total bone content were significantly reduced in *Plcg2*$^{Ali14/+}$ mice of both sexes (results available at http://abe.med.u-tokai.ac.jp/index.html or from the corresponding author upon request). This was mainly due to a significant reduction in trabecular bone density and cortical bone content. Concurrently, the trabecular bone area was increased, whereas the cortical bone area was reduced.

In addition to the bone defects, male *Plcg2*$^{Ali14/+}$ mice showed a significantly reduced fat mass, as revealed by DXA (Figure 4C). Although DXA analysis of fat mass is, unlike other methods, a semiquantitative approach, the significant reduction in body weight observed in male *Plcg2*$^{Ali14/+}$ mice (Figure 4D) strongly supports the notion that body fat is reduced in *Plcg2*$^{Ali14/+}$ mice. NMR analysis of the body composition of *Plcg2*$^{Ali14/+}$ mice confirmed this notion; male *Plcg2*$^{Ali14/+}$ mice exhibited significantly reduced fat mass (mean ± SEM 6.5 ± 0.8 units in *Plcg2*$^{Ali14/+}$ mice versus 8.4 ± 1.4 units in WT mice; $P < 0.005$) and reduced lean mass (19.6 ± 1.3 units in *Plcg2*$^{Ali14/+}$ mice versus 21.6 ± 0.7 units in WT mice; $P < 0.01$). In male *Plcg2*$^{Ali14/+}$ mice, we detected a significant genotype effect on the relationship between body mass and fat mass content. Interestingly, female *Plcg2*$^{Ali14/+}$ mice also showed tendencies toward having reduced fat mass and reduced body weight (Figures 4C and D), but this was not observed in the batch of mice used for NMR analysis.

**Novel phenotypes identified by plasma biochemical screening.** In the German Mouse Clinic (28), we screened various biochemical plasma parameters to identify novel phenotypes in *Plcg2*$^{Ali14/+}$ mice. Of the 20 parameters measured in the clinical chemical screening, the values for cholesterol, triglycerides, and alkaline phosphatase were found to be abnormal in *Plcg2*$^{Ali14/+}$ mouse plasma (Table 1). In male *Plcg2*$^{Ali14/+}$ mice, the mean value for cholesterol was 2.8 m*M*, which was 1.5 m*M* lower than that in WT mouse plasma. Female *Plcg2*$^{Ali14/+}$ mice also had a slightly lower concentration of cholesterol (mean 2.4 m*M* in female *Plcg2*$^{Ali14/+}$ mice versus 2.9 m*M* in female WT mice). The between-group differences in this parameter were significant in both male *Plcg2*$^{Ali14/+}$ mice and female *Plcg2*$^{Ali14/+}$ mice, as determined by Welch's *t*-test ($P < 0.001$ in males and $P < 0.01$ in females, versus WT mice).

With regard to peripheral triglyceride levels, *Plcg2*$^{Ali14/+}$ mice showed significantly lower concentrations than were observed in WT mice (mean 2.7 m*M* and 1.9 m*M* in male and female *Plcg2*$^{Ali14/+}$ mice, respectively versus 4.3 m*M* and 2.8 m*M* in male and female WT mice, respectively). Alkaline phosphatase activity was found to be significantly reduced in both male and female *Plcg2*$^{Ali14/+}$ mice (mean 66.3 units/liter and 122.9 units/liter in male and female *Plcg2*$^{Ali14/+}$ mice, respectively versus 96.9 units/liter and 142.4 units/liter in male and female WT mice, respectively). Blood glucose values were significantly reduced only in male mice of the *Plcg2*$^{Ali14/+}$ strain (97.9 mg/dl in male *Plcg2*$^{Ali14/+}$ mice versus 131.3 mg/dl in male WT mice). In the steroid metabolism screening, significantly reduced levels of

**Table 1.** Results of laboratory chemical analyses of blood plasma from *Plcg2*$^{Ali14/+}$ mice*

| Parameter | Male | | | Female | | |
|---|---|---|---|---|---|---|
| | Wild-type (n = 7) | *Plcg2*$^{Ali14/+}$ (n = 8) | *P* | Wild-type (n = 10) | *Plcg2*$^{Ali14/+}$ (n = 11) | *P* |
| Albumin, gm/liter | 26.3 ± 0.52 | 24.3 ± 0.25 | <0.01 | 27.2 ± 0.43 | 25.8 ± 0.18 | <0.05 |
| Urea, m*M* | 10.3 ± 0.30 | 9.0 ± 0.17 | <0.01 | 9.4 ± 0.41 | 8.3 ± 0.26 | <0.05 |
| Cholesterol, m*M* | 4.3 ± 0.14 | 2.8 ± 0.13 | <0.001 | 2.9 ± 0.09 | 2.4 ± 0.05 | <0.01 |
| Triglycerides, m*M* | 4.3 ± 0.29 | 2.7 ± 0.30 | <0.01 | 2.8 ± 0.14 | 1.9 ± 0.20 | <0.01 |
| AP, units/liter | 96.9 ± 1.99 | 66.3 ± 4.83 | <0.001 | 142.4 ± 6.41 | 122.9 ± 4.05 | <0.05 |
| Glucose, mg/dl | 131.3 ± 8.2 | 97.9 ± 8.7 | <0.05 | 118.8 ± 7.5 | 128.5 ± 5.2 | NS |
| DHEA, pg/ml | 127.0 | 35.4 | <0.01 | 94.0 | 91.8 | NS |

* Values are the mean ± SEM. The parameters selected were those in which a significant difference between groups was found on duplicate tests performed 3 weeks apart. AP = alkaline phosphatase; NS = not significant; DHEA = dehydroepiandrosterone.

dehydroepiandrosterone (DHEA) were detected only in male *Plcg2*$^{Ali14/+}$ mice (mean 35.4 pg/ml versus 127.0 pg/ml in male WT mice; $P < 0.01$).

**Normal sperm motility, but impaired IVF ability, in male *Plcg2*$^{Ali14/+}$ mice.** Although the mutation was transmitted to the next generation at a normal rate by natural mating (results not shown), we found that spermatozoa from male *Plcg2*$^{Ali14/+}$ mice failed to achieve fertilization in vitro. Table 2 shows a summary of the findings from IVF experiments using spermatozoa from *Plcg2*$^{Ali14/+}$ mice, performed using a standard procedure as described in Materials and Methods. Notably, the 2-cell cleavage rate of *Plcg2*$^{Ali14/+}$ mouse spermatozoa was less than 5% (Table 2). Overall, we used 1,959 oocytes, but only 16 embryos were developed using *Plcg2*$^{Ali14/+}$ mouse spermatozoa (0.8%). In contrast, in experiments using WT mouse spermatozoa, 82.1% of 262 oocytes developed to 2-cell stage embryos. However, the motility and progressivity of sperm from *Plcg2*$^{Ali14/+}$ mice were comparable with those of WT mouse sperm (results available at http://abe.med.u-tokai.ac.jp/index.html or from the corresponding author upon request).

## DISCUSSION

In this study, we identified a novel dominant mutation, *Ali14*, causing spontaneous inflammation of the peripheral paws of mice. From genetic mapping analysis and candidate sequencing, we identified an AT-to-GC transition in the coding region of *Plcg2*. Furthermore, additional phenotypes of *Plcg2*$^{Ali14/+}$ mice were analyzed intensively in a systematic phenotyping center, the German Mouse Clinic (28,29). After analyzing more than 240 parameters in this study, we found novel functions of *Plcg2* in vivo. This detailed phenotype description gives insights into the hidden roles of PLC signaling in vivo.

A line of experimental evidence indicates that the *Ali14* mutation is a gain-of-function mutation of *Plcg2*. *Plcg2* catalyzes formation of the second messengers, $IP_3$

**Table 2.** Results of in vitro fertilization (IVF) experiments using sperm from male *Plcg2*$^{Ali14/+}$ mice*

| IVF experiment | Parental strain | | No. of oocytes | No. of 2-cell embryos | Cleavage rate, % |
|---|---|---|---|---|---|
| | Male | Female | | | |
| 1 | *Plcg2*$^{Ali14/+}$ | Wild-type | 450 | 0 | 0.0 |
| 2 | *Plcg2*$^{Ali14/+}$ | Wild-type | 322 | 14 | 4.3 |
| 3 | *Plcg2*$^{Ali14/+}$ | Wild-type | 468 | 0 | 0.0 |
| 4 | *Plcg2*$^{Ali14/+}$ | Wild-type | 455 | 2 | 0.4 |
| 5 | *Plcg2*$^{Ali14/+}$ | Wild-type | 264 | 0 | 0.0 |
| 6 | Wild-type | Wild-type | 67 | 52 | 77.6 |
| 7 | Wild-type | Wild-type | 150 | 130 | 86.7 |
| 8 | Wild-type | Wild-type | 45 | 33 | 73.3 |
| Total | | | | | |
| *Plcg2*$^{Ali14/+}$ sperm | | | 1,959 | 16 | 0.8 |
| Wild-type sperm | | | 262 | 215 | 82.1 |

* *Plcg2*$^{Ali14/+}$ mice (C3HeB/FeJ [C3H] background) and C3H wild-type mice were used for IVF experiments. In all experiments, fresh spermatozoa from different mice were used.

and DAG. $IP_3$ mediates release of intracellular $Ca^{2+}$ from the endoplasmic reticulum, and the increased concentration of $Ca^{2+}$ then returns to the basal level for a certain time. The cultured cells expressing *Ali14-Plcg2* proteins exhibited a high initial peak of $Ca^{2+}$ concentration and a prolonged return-to-basal time (Figure 3C), suggesting that *Plcg2*-mediated signals are enhanced more in *Plcg2*$^{Ali14/+}$ mice. The *Ali14* mutation causes an amino acid substitution in an spPH domain of *Plcg2*. PH domains function as structural modules for membrane association and protein–protein interaction involving inosito-lipid–mediated intracellular signaling (30). Recently, it was reported that Rac GTPases cause marked stimulation of *Plcg2* (31). Furthermore, this stimulation is regulated by interaction between Rac and the spPH domains of *Plcg2* (32). Our previous results indicated that the *Ali14-Plcg2* protein enhances Rac activation of *Plcg2* without increasing Rac binding, and also enhances the response to EGF stimulation (27). Therefore, *Ali14*-mutated proteins affect basal enzymatic activity slightly but amplify signals more strongly than WT proteins. Taken together, these findings strongly indicate that the *Ali14* mutation is a gain-of-function allele of *Plcg2*.

Abnormalities in the adoptive immune system of *Plcg2*$^{Ali14/+}$ mice are similar to the phenotypes of *Plcg2*$^{Ali5/+}$ mice. In the mouse peripheral blood, in addition to an abnormal T cell:B cell ratio, up-regulation of IgM and IgG1 is identical between *Plcg2*$^{Ali14/+}$ mice and *Plcg2*$^{Ali5/+}$ mice (16). In contrast, *Plcg2*-knockout mice show decreased IgM levels and do not show an induction of an increase in intracellular $Ca^{2+}$ in B cells (9,33). The increased populations of T cells in *Plcg2*$^{Ali14/+}$ mice must be secondary effects, because *Plcg1* predominates in T cells (7). Results of analysis of T cells in *Plcg2*$^{Ali5/+}$ mice support this notion, in that *Ali5* T cells do not exhibit an enhanced $Ca^{2+}$ response by T cell receptor stimulation (16).

Transfer of bone marrow cells from *Plcg2*$^{Ali5/+}$ mice results in reconstitution of inflammatory arthritis in irradiated WT mice. However, *Plcg2*$^{Ali5/+}$ mice with a double mutation of *RAG2* (*RAG2*-knockout allele), which lack mature lymphocytes, show the arthritis phenotype (16). Overall, bone marrow–derived cells are responsible for the phenotype, but lymphocytes are not essential to trigger inflammation in *Plcg2*$^{Ali5/+}$ mice. Similarly, the adoptive transfer experiments in this study revealed that a certain number of *Ali14*/+ splenocytes, most of which consist of lymphocytes, contribute very little to arthritis induction. Therefore, it is most likely that the functions of lymphocytes, including autoreactive T cell responses and autoantibodies, are not involved in the initial phase of arthritis in *Ali14*/+ mice.

In *Plcg2*-deficient mice, a loss of collagen-induced platelet aggregation, impaired degranulation of mast cells, and dysfunction of NK cells were observed (9). Furthermore, *Plcg2* is involved in neutrophil activation and neutrophil-mediated arthritis induction in the K/BxN serum-transfer model (34,35). Mast cells and neutrophils are mostly derived from bone marrow and circulate in the peripheral blood. However, they seldom stay in lymphoid organs, such as the spleen. This life cycle is suitable for explaining the pathogenesis of arthritis in *Ali14*/+ mice. Thus, it is interesting to analyze the myeloid-lineage cells as candidates for a primary trigger of spontaneous inflammation in *Plcg2*$^{Ali5/+}$ and *Plcg2*$^{Ali14/+}$ mice.

Using DXA and peripheral QCT analyses, we found a significant decrease in the bone mineral content and bone mineral density in *Plcg2*$^{Ali14/+}$ mice. *Plcg2*-knockout mice have been found to have an osteopetrotic phenotype because of the decrease in the number of osteoclasts in these mice (36), suggesting that *Plcg2*-mediated signals are necessary for osteoclast formation. Therefore, it is important to analyze whether factors downstream of *Plcg2* signaling, such as nuclear factor of activated T cells and NF-κB, are active in osteoclasts in *Plcg2*$^{Ali14/+}$ mice. It is likely that both constitutive osteoclast activation and decreased bone formation lead to the osteoporotic phenotype in *Plcg2*$^{Ali14/+}$ mice. Further analyses using biomarkers of bone formation and resorption are necessary to depict molecular mechanisms of bone defects in *Plcg2*$^{Ali14/+}$ mice.

In female *Plcg2*$^{Ali14/+}$ mice, swollen paws are rarely detected in our rearing system. This difference between sexes is also obvious in *Ali5*/+ mice, despite the fact there is no between-sex difference in lymphocyte abnormality (16). We hypothesize that regulation of sex hormones may be related to the modification of the arthritis phenotype in *Ali14*/+ mice. The results from the steroid hormone screen support this notion, in that DHEA levels were reduced only in male *Ali14*/+-heterozygous mice (Table 1). The testosterone concentration was also reduced in male mice, although a statistically significant difference was not detected (results not shown). Androgens are able to inhibit cutaneous wound healing, possibly by modulating inflammatory responses (37,38). This unknown mechanism may be involved in inflammatory responses via the *Plcg2*-mediated signaling cascade.

The rate of IVF using spermatozoa from *Plcg2*$^{Ali14/+}$ mice was extremely low, despite normal

sperm motility and progressivity in these mice (Table 2 and results not shown). This indicates that not only *Ali14*, but also WT (+) haploid sperm from *Plcg2*$^{Ali14/+}$ mice showed impaired fertility in vitro. The WT haploid spermatozoa in *Plcg2*$^{Ali14/+}$ mice might contain mutant *Plcg2*$^{Ali14}$ proteins, since all of the spermatozoa are originated from diploid spermatogonial (*Ali14*/+) stem cells. If the *Plcg2* proteins were produced in spermatogenesis and accumulated in the cytoplasm, all mature spermatozoa in *Ali14*/+ mice share the mutant proteins. This may also explain the complete sterility of *Plcg2*$^{Ali5/+}$ mice (16). Because *Plcg2*$^{Ali14/+}$ mice show normal fertility in vivo, once fertilization occurs, the *Plcg2* pathways are not essential for further development. Therefore, we speculate that the *Plcg2*-mediated pathway might be involved in the acrosome reaction, but not in the zygote formation. PLCs are actually activated during sperm capacitation (39). Furthermore, $Ca^{2+}$ oscillation and *Plcg* are tightly linked in the acrosome reaction (40). Therefore, it would be worthwhile to visualize the acrosome reaction and calcium mobilization using fluorescent molecular probes in *Ali14* and *Ali5* spermatozoa.

Using simplified methods, we detected a reduction in body weight and fat mass only in male *Plcg2*$^{Ali14/+}$ mice. NMR analysis of *Plcg2*$^{Ali14/+}$ mice confirmed this male-specific reduction in fat and lean mass in quantitative levels (results available from the corresponding author upon request). In addition, the concentration of peripheral triglycerides was also significantly decreased in male heterozygotes. Since only male heterozygous mice show the arthritis phenotype in our rearing system, the reduction in fat mass could be a consequence of spontaneous inflammation induced by the *Ali14* mutation. In humans, cachexia is characterized by weight loss that involves depletion of host adipose tissue and skeletal muscle mass (2). It occurs with a number of diseases, including cancer, acquired immunodeficiency syndrome, and major trauma.

Rheumatoid cachexia is characterized by reduced body cell mass in patients with rheumatoid arthritis (41). Cachexia-like phenotypes were also found in animal models of inflammatory arthritis; human tumor necrosis factor $\alpha$ (TNF$\alpha$)–transgenic mice show weight loss, as well as a reduction in fat and lean mass (42). This line of evidence strongly suggests that cachexia is related to increased levels of TNF$\alpha$. Although there has been no direct evidence to support the notion of an interaction between TNF$\alpha$ and *Plcg2*, a number of reports indicate a possibility of the interaction. In bone marrow–derived macrophages, *Plcg2* is necessary for full production of TNF$\alpha$, because TNF$\alpha$ levels induced by lipopolysaccharide are clearly reduced in *Plcg2* conditional-knockout mice (43). In humans, TNF$\alpha$ induces cyclooxygenase 2 in lung epithelial cells. However, this induction is strongly attenuated by U73122, a general inhibitor of PLCs (44). Thus, *Plcg2* is a key molecule in TNF$\alpha$-mediated signaling in lung epithelial cells. Therefore, it is likely that a gain-of-function mutation in *Plcg2* results in the cachexia-like phenotype, via overproduction of TNF$\alpha$ or activation of the TNF$\alpha$-mediated pathways.

In the present study, we have thus characterized a novel ENU-induced dominant mutation, *Ali14*, whose phenotype presents as swollen peripheral limbs. By genetic mapping and candidate sequencing, we identified *Ali14* as a missense mutation in *Plcg2*. In addition to inflammatory infiltrates in the paws, we found various metabolic defects in *Ali14* heterozygous mice by systematic phenotyping. Furthermore, IVF experiments with spermatozoa from *Ali14* heterozygotes resulted in extremely low IVF rates, despite the normal fertility of the heterozygous mice in vivo. Recently, we obtained *Ali14* homozygous mice, which exhibit much more severe arthritis and an earlier onset of arthritis, at ~3 weeks of age, in both sexes. This preliminary study indicated that *Ali14* is a semidominant mutation; it is predicted that the compound-mutant mice with *Ali14* and a knockout allele (*Ali14*/−) show phenotypes similar to those of *Ali14* homozygous (*Ali14*/*Ali14*) mice. Since the homozygous mice do not show diminished survival rates (they survive long enough to reach sexual maturity), the metabolic abnormality and fertility, as well as inflammatory arthritis phenotype, in these mice can be compared with those of heterozygotes. These findings could extend the understanding of the complex molecular effects of inflammation to a whole body, such as that observed in rheumatoid cachexia.

## ACKNOWLEDGMENTS

We gratefully acknowledge the excellent technical assistance of Michael Schulz, Reinhard Seeliger, Sabrina Bothur, Michaela Grandl, Elfie Holupierek, Katrin Laube, Jacqueline Mueller, Elenore Samson, Florian Schleicher, Daniela Schmidt, Waldemar Schneider, Ann-Elisabeth Schwarz, Lucie Thurmann, and Susanne Wittich, as well as all members of the ENU core facility and the animal caretaker team. We also thank the members of the German Mouse Clinic for comprehensive phenotyping and discussions.

## AUTHOR CONTRIBUTIONS

All authors were involved in drafting the article or revising it critically for important intellectual content, and all authors approved the final version to be published. Dr. Abe had full access to all of the

data in the study and takes responsibility for the integrity of the data and the accuracy of the data analysis.

**Study conception and design.** Abe, Fuchs, Boersma, Hans, Yu, Rathkolb, Rozman, Esposito, Klingenspor, Wurst, Gailus-Durner, Marschall, Soewarto, Wagner, Hrabě de Angelis.

**Acquisition of data.** Abe, Boersma, Hans, Yu, Kalaydjiev, Klaften, Mossbrugger, Rathkolb, Rozman, Prehn, Maraslioglu, Kametani, Shimada, Adamski, Esposito, Klingenspor, Wolf, Gailus-Durner, Soewarto, Wagner.

**Analysis and interpretation of data.** Abe, Fuchs, Boersma, Hans, Yu, Kalaydjiev, Klaften, Adler, Calzada-Wack, Mossbrugger, Rathkolb, Rozman, Prehn, Maraslioglu, Kametani, Shimada, Adamski, Busch, Esposito, Klingenspor, Katan, Wagner, Hrabě de Angelis.

## REFERENCES


1. Firestein GS, Budd RC, Harris ED Jr, McInnes IB, Ruddy S, Sergent JS. Kelley's textbook of rheumatology. 8th ed. Philadelphia: Saunders; 2008.
2. Tisdale MJ. Biology of cachexia. J Natl Cancer Inst 1997;89: 1763–73.
3. Suh PG, Park JI, Manzoli L, Cocco L, Peak JC, Katan M, et al. Multiple roles of phosphoinositide-specific phospholipase C isozymes. BMB Rep 2008;41:415–34.
4. Majerus PW, Connolly TM, Deckmyn H, Ross TS, Bross TE, Ishii H, et al. The metabolism of phosphoinositide-derived messenger molecules. Science 1986;234:1519–26.
5. Ji QS, Winnier GE, Niswender KD, Horstman D, Wisdom R, Magnuson MA, et al. Essential role of the tyrosine kinase substrate phospholipase C-γ1 in mammalian growth and development. Proc Natl Acad Sci U S A 1997;94:2999–3003.
6. Kurosaki T, Maeda A, Ishiai M, Hashimoto A, Inabe K, Takata M. Regulation of the phospholipase C-γ2 pathway in B cells. Immunol Rev 2000;176:19–29.
7. Wilde JI, Watson SP. Regulation of phospholipase Cγ isoforms in haematopoietic cells: why one, not the other? Cell Signal 2001;13: 691–701.
8. Satterthwaite AB, Li Z, Witte ON. Btk function in B cell development and response. Semin Immunol 1998;10:309–16.
9. Wang D, Feng J, Wen R, Marine JC, Sangster MY, Parganas E, et al. Phospholipase Cγ2 is essential in the functions of B cell and several Fc receptors. Immunity 2000;13:25–35.
10. Ichise H, Ichise T, Ohtani O, Yoshida N. Phospholipase Cγ2 is necessary for separation of blood and lymphatic vasculature in mice. Development 2009;136:191–5.
11. Soewarto D, Klaften M, Rubio-Aliaga I. Features and strategies of ENU mouse mutagenesis. Curr Pharm Biotechnol 2009;10: 198–213.
12. Hrabe de Angelis MH, Flaswinkel H, Fuchs H, Rathkolb B, Soewarto D, Marschall S, et al. Genome-wide, large-scale production of mutant mice by ENU mutagenesis. Nat Genet 2000;25: 444–7.
13. Fuchs H, Schughart K, Wolf E, Balling R, Hrabe de Angelis M. Screening for dysmorphological abnormalities: a powerful tool to isolate new mouse mutants. Mamm Genome 2000;11:528–30.
14. Soewarto D, Fella C, Teubner A, Rathkolb B, Pargent W, Heffner S, et al. The large-scale Munich ENU-mouse-mutagenesis screen. Mamm Genome 2000;11:507–10.
15. Nadeau JH. Modifier genes in mice and humans. Nat Rev Genet 2001;2:165–74.
16. Yu P, Constien R, Dear N, Katan M, Hanke P, Bunney TD, et al. Autoimmunity and inflammation due to a gain-of-function mutation in phospholipase Cγ2 that specifically increases external $Ca^{2+}$ entry. Immunity 2005;22:451–65.
17. Abe K, Fuchs H, Lisse T, Hans W, Hrabe de Angelis M. New ENU-induced semidominant mutation, Ali18, causes inflammatory arthritis, dermatitis, and osteoporosis in the mouse. Mamm Genome 2006;17:915–26.
18. Abe K, Wechs S, Kalaydjiev S, Franz TJ, Busch DH, Fuchs H, et al. Novel lymphocyte-independent mechanisms to initiate inflammatory arthritis via bone marrow-derived cells of Ali18 mutant mice. Rheumatology (Oxford) 2008;47:292–300.
19. Abe K, Klaften M, Narita A, Kimura T, Imai K, Kimura M, et al. Genome-wide search for genes that modulate inflammatory arthritis caused by Ali18 mutation in mice. Mamm Genome 2009; 20:152–61.
20. Abe K, Yu P. Positional cloning in mice and its use for molecular dissection of inflammatory arthritis. Curr Pharm Biotechnol 2009; 10:252–60.
21. Kunder S, Calzada-Wack J, Hoelzlwimmer G, Mueller J, Kloss C, Howat W, et al. A comprehensive antibody panel for immunohistochemical analysis of formalin-fixed, paraffin-embedded hematopoietic neoplasms of mice: analysis of mouse specific and human antibodies cross-reactive with murine tissue. Toxicol Pathol 2007; 35:366–75.
22. Kalaydjiev S, Franz T, Busch D. Mouse phenotyping: immunology. In: Hrabe de Angelis M, Chambon P, Brown SD, editors. Standards of mouse model phenotyping. Weinheim (Germany): WILEY-VCH Verlag; 2006. p. 237–52.
23. Fuchs H, Lisse T, Abe K, Hrabe de Angelis M. Screening for bone and cartilage phenotypes in mice. In: Hrabe de Angelis M, Chambon P, Brown SD, editors. Standards of mouse model phenotyping. Weinheim (Germany): WILEY-VCH Verlag; 2006. p. 35–86.
24. Fuchs H, Lisse T, Hans W, Abe K, Thiele F, Gailus-Durner V, et al. Phenotypic characterization of mouse models for bone-related diseases in the German Mouse Clinic. J Musculoskelet Neuronal Interact 2008;8:13–4.
25. Marschall S, Boersma A, Hrabe de Angelis M. Sperm cryopreservation and in vitro fertilization. Methods Mol Biol 2009;530: 407–20.
26. Schneider M, Forster H, Boersma A, Seiler A, Wehnes H, Sinowatz F, et al. Mitochondrial glutathione peroxidase 4 disruption causes male infertility. FASEB J 2009;23:3233–42.
27. Everett KL, Bunney TD, Yoon Y, Rodrigues-Lima F, Harris R, Driscoll PC, et al. Characterization of phospholipase Cγ enzymes with gain-of-function mutations. J Biol Chem 2009;284:23083–93.
28. Fuchs H, Gailus-Durner V, Adler T, Pimentel JA, Becker L, Bolle I, et al. The German Mouse Clinic: a platform for systemic phenotype analysis of mouse models. Curr Pharm Biotechnol 2009;10:236–43.
29. Gailus-Durner V, Fuchs H, Becker L, Bolle I, Brielmeier M, Calzada-Wack J, et al. Introducing the German Mouse Clinic: open access platform for standardized phenotyping. Nat Methods 2005;2:403–4.
30. Ferguson KM, Lemmon MA, Schlessinger J, Sigler PB. Structure of the high affinity complex of inositol trisphosphate with a phospholipase C pleckstrin homology domain. Cell 1995;83:1037–46.
31. Piechulek T, Rehlen T, Walliser C, Vatter P, Moepps B, Gierschik P. Isozyme-specific stimulation of phospholipase C-γ2 by Rac GTPases. J Biol Chem 2005;280:38923–31.
32. Walliser C, Retlich M, Harris R, Everett KL, Josephs MB, Vatter P, et al. Rac regulates its effector phospholipase Cγ2 through interaction with a split pleckstrin homology domain. J Biol Chem 2008;283:30351–62.
33. Hashimoto A, Takeda K, Inaba M, Sekimata M, Kaisho T, Ikehara S, et al. Cutting edge: essential role of phospholipase C-γ2 in B cell development and function. J Immunol 2000;165:1738–42.
34. Cremasco V, Graham DB, Novack DV, Swat W, Faccio R. Vav/phospholipase Cγ2–mediated control of a neutrophil-

dependent murine model of rheumatoid arthritis. Arthritis Rheum 2008;58:2712–22.
35. Jakus Z, Simon E, Frommhold D, Sperandio M, Mocsai A. Critical role of phospholipase Cγ2 in integrin and Fc receptor-mediated neutrophil functions and the effector phase of autoimmune arthritis. J Exp Med 2009;206:577–93.
36. Mao D, Epple H, Uthgenannt B, Novack DV, Faccio R. PLCγ2 regulates osteoclastogenesis via its interaction with ITAM proteins and GAB2. J Clin Invest 2006;116:2869–79.
37. Ashcroft GS, Mills SJ. Androgen receptor-mediated inhibition of cutaneous wound healing. J Clin Invest 2002;110:615–24.
38. Lai JJ, Lai KP, Chuang KH, Chang P, Yu IC, Lin WJ, et al. Monocyte/macrophage androgen receptor suppresses cutaneous wound healing in mice by enhancing local TNF-α expression. J Clin Invest 2009;119:3739–51.
39. Spungin B, Margalit I, Breitbart H. Sperm exocytosis reconstructed in a cell-free system: evidence for the involvement of phospholipase C and actin filaments in membrane fusion. J Cell Sci 1995;108:2525–35.
40. Breitbart H. Intracellular calcium regulation in sperm capacitation and acrosomal reaction. Mol Cell Endocrinol 2002;187:139–44.
41. Roubenoff R, Roubenoff RA, Cannon JG, Kehayias JJ, Zhuang H, Dawson-Hughes B, et al. Rheumatoid cachexia: cytokine-driven hypermetabolism accompanying reduced body cell mass in chronic inflammation. J Clin Invest 1994;93:2379–86.
42. Hayward MD, Jones BK, Saparov A, Hain HS, Trillat AC, Bunzel MM, et al. An extensive phenotypic characterization of the hTNFα transgenic mice. BMC Physiol 2007;7:13.
43. Aki D, Minoda Y, Yoshida H, Watanabe S, Yoshida R, Takaesu G, et al. Peptidoglycan and lipopolysaccharide activate PLCγ2, leading to enhanced cytokine production in macrophages and dendritic cells. Genes Cells 2008;13:199–208.
44. Chen CC, Sun YT, Chen JJ, Chiu KT. TNF-α-induced cyclooxygenase-2 expression in human lung epithelial cells: involvement of the phospholipase C-γ2, protein kinase C-α, tyrosine kinase, NF-κB-inducing kinase, and I-κB kinase 1/2 pathway. J Immunol 2000;165:2719–28.

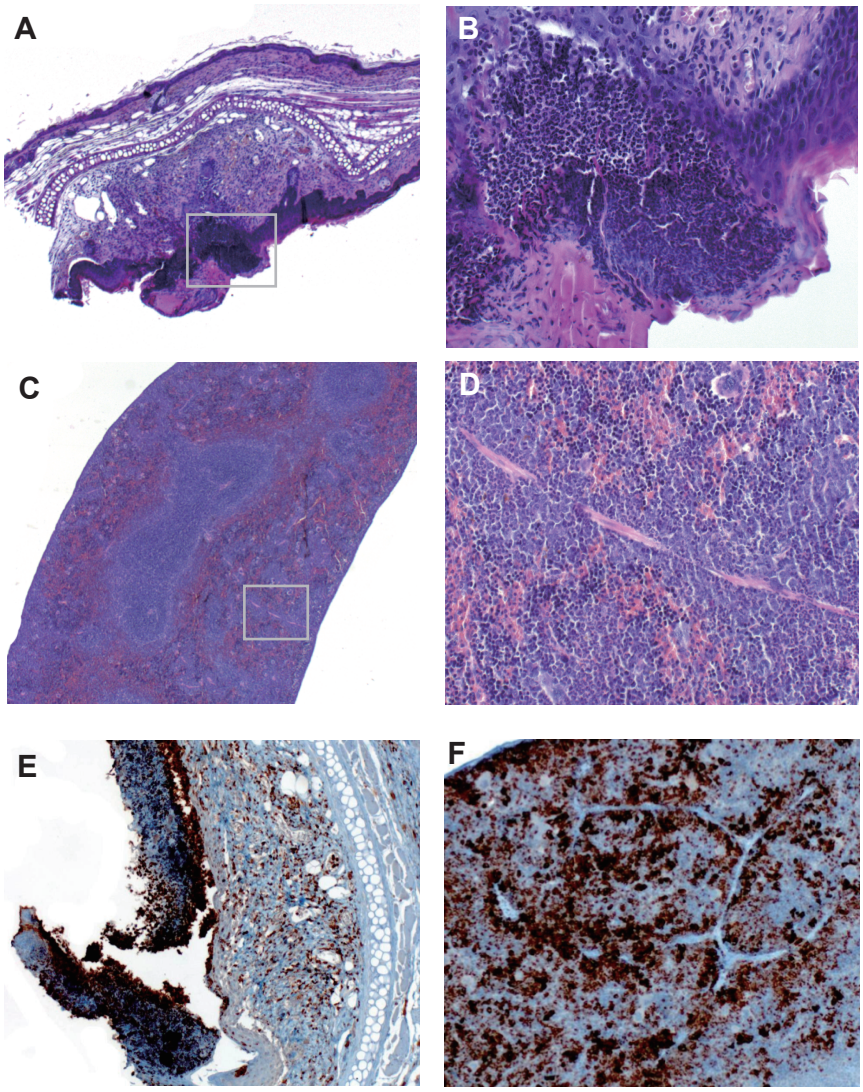


**Supplementary Figure 1.** (G, H) HE staining of sections from auricles of *Ali14/+* mice. Ulceration and infiltration of inflammatory cells in dermis were observed. (I, H) HE staining of sections of *Ali14/+* spleen. Proliferation of granulocytes was observed in red pulp. Immunohistochemistry using anti-myeloperoxidase antibodies revealed majority of inflammatory cells in the auricle (K) and the spleen (L) were granulocytes. (H) and (J) are magnification of insets in (G) and (I), respectively. Original magnification: (G) and (I), x12.5; (H) and (J), x200; (K) and (L), x100.

**Supplementary Table 1.** Peripheral quantitative computed tomography (pQCT) analysis of femoral metaphysis in *Plcg2*$^{Ali14/+}$ mice

| | Male (n) | | | Female (n) | | |
|---|---|---|---|---|---|---|
| Parameter | *wild type* (10) | *Plcg2*$^{Ali14/+}$ (9) | *P*-value | *wild type* (10) | *Plcg2*$^{Ali14/+}$ (10) | *P*-value |
| Total density (mg/cm$^3$) | 616±5 | 580±5 | <0.005 | 744±8 | 692±7 | <0.005 |
| Trabecular density (mg/cm$^3$) | 294±4 | 273±6 | <0.005 | 296±6 | 255±5 | <0.005 |
| Cortical density (mg/cm$^3$) | 823±6 | 809±7 | n.s. | 887±8 | 873±7 | n.s. |
| Total contents (mg) | 2.12±0.02 | 2.02±0.01 | <0.005 | 2.35±0.03 | 2.21±0.03 | <0.005 |
| Trabecular contents (mg) | 0.40±0.01 | 0.41±0.01 | n.s. | 0.22±0.01 | 0.24±0.01 | n.s. |
| Cortical contents (mg) | 1.72±0.02 | 1.61±0.01 | <0.005 | 2.13±0.03 | 1.98±0.03 | <0.005 |
| Total area (mm$^2$) | 3.44±0.04 | 3.48±0.04 | n.s. | 3.17±0.04 | 3.2-±0.03 | n.s. |
| Trabecular area (mm$^2$) | 1.35±0.03 | 1.49±0.03 | <0.005 | 0.76±0.03 | 0.93±0.03 | <0.005 |
| Cortical area (mm$^2$) | 2.10±0.03 | 1.99±0.02 | <0.05 | 2.41±0.05 | 2.26±0.04 | <0.05 |

The pQCT data from 16-weeks-old mice were presented as mean ± standard error of mean. Statistical analysis was performed by unpaired Student's *t* test.

**Supplementary Table 2.** Nuclear Magnetic Resonance (NMR) analysis of *Plcg2*$^{Ali14/+}$ mice

| Sex | Genotype (n) | Body mass (g) | *P*-value | Fat mass (g) | *P*-value | Lean mass (g) | *P*-value |
|---|---|---|---|---|---|---|---|
| Male | *wild type* (10) | 34.8±1.8 | – | 8.4±1.4 | – | 21.6±0.7 | – |
| | *Plcg2*$^{Ali14/+}$ (10) | 30.9±2.1 | <0.001 | 6.5±0.8 | <0.005 | 19.6±1.3 | <0.001 |
| Female | *wild type* (10) | 30.4±2.6 | – | 8.5±1.6 | – | 17.7±1.1 | – |
| | *Plcg2*$^{Ali14/+}$ (10) | 30.8±3.6 | n.s. | 8.8±2.3 | n.s. | 18.6±1.6 | n.s. |

Fat and lean mass were compared using a linear model including body mass as covariate.

**Supplementary Table 3.** Sperm quality measuremnets using sperm analyzer

| Strain | Number of males | Motility (%) | *P*-value | Progressivity (%) | *P*-value |
|---|---|---|---|---|---|
| *wild type* | 20 | 69.0±15.2 | - | 36.7±12.0 | - |
| *Plcg2*$^{Ali14/+}$ | 12 | 77.4±10.4 | 0.16 (n.s.) | 43.5±7.8 | 0.12 (n.s.) |

Wilcoxon rank-sum test was used for statistical significance. Mean±SEM is shown.